

Spin correlation and relaxational dynamics in molecular-based single-chain magnets

Jun-ichiro Kishine,^{1,2} Tomonari Watanabe,¹ Hiroyuki Deguchi,^{1,2} Masaki Mito,^{1,2} Tôru Sakai,^{2,3} Takayuki Tajiri,¹ Masahiro Yamashita,^{2,4} and Hitoshi Miyasaka^{2,4,5}¹Faculty of Engineering, Kyushu Institute of Technology, Kitakyushu 804-8550, Japan²CREST, Japan Science and Technology Agency (JST), Saitama 332-0012, Japan³Japan Atomic Energy Research Institute (JAERI), SPring-8, Mikazuki, Hyogo 679-5148, Japan⁴Department of Chemistry, Tohoku University, Sendai 980-8578, Japan⁵PRESTO, Japan Science and Technology Agency (JST), Saitama 332-0012, Japan

(Received 31 May 2006; revised manuscript received 21 September 2006; published 15 December 2006)

We report the combined measurements of the dc susceptibility χ_0 , the ac susceptibility χ' , and the NMR relaxation rate T_1^{-1} for the molecular-based heterometallic single-chain magnet $[\text{Mn}(\text{saltmen})_2[\text{Ni}(\text{pao})_2(\text{py})_2](\text{PF}_6)_2$. At low temperatures, this system is well described by a one-dimensional array of effective spin $S=3$ chains comprising the $\text{Mn}^{\text{III}}\text{-Ni}^{\text{II}}\text{-Mn}^{\text{III}}$ trimers and treated as the $S=3$ Ising chain with the single-ion term (Blume-Capel model). Using the exact solution of the model and based on the picture that the random motion of the local domain walls dominates the low-temperature spin dynamics, we succeeded in reproducing the experimental results of the dc susceptibility χ_0 , the ac susceptibility χ' , and the ^{19}F -NMR relaxation rate T_1^{-1} in a consistent manner.

DOI: 10.1103/PhysRevB.74.224419

PACS number(s): 75.40.Gb, 75.10.Pq, 75.50.Xx, 76.90.+d

I. INTRODUCTION

Nonequilibrium dynamics in critical phenomena has been studied for a long time as a fundamental problem of statistical physics. Central to the issue is to understand long-time and large-scale fluctuations near the phase transition point.¹ One-dimensional (1D) *classical* spin systems provide canonical examples to study this problem, since the 1D classical systems become critical toward zero temperature. Then, the characteristic time scale to flip the correlated domains is governed by the correlation length ξ . Glauber highlighted this problem based on the kinetic Ising model coupled to a heat bath where the stochastic dynamics is triggered by single spin flips.² Elementary excitations of the Ising ferromagnet are described by spin cluster excitations (SCE's) surrounded by local domain walls, which have detectable through electron spin resonance spectra.³ The domain wall (DW) motion costs no energy, and consequently the relaxation process is determined by the random motion of the DW's. This process gives rise to nonconserved dynamics and leads to the relaxation time $\tau \propto \xi^z$, with the dynamical exponent $z=2$.¹

To elucidate the slow dynamics of the low-dimensional spin systems in real materials with or without the Ising anisotropy has been a target of intensive research since the 1970s.^{4,5} In particular, the diffusive dynamics of the one-dimensional Heisenberg system TMMC has been scrutinized as a canonical example of the 1D spin system. In the 1D Heisenberg system, conservation of the order parameter leads the diffusive spin dynamics.^{1,4,5} NMR measurements on the spin dynamics have also been done for this system.⁶ Similar work exists for the ferromagnet CsNiF_3 .⁷ Even compiling these works, it is still a highly nontrivial issue whether the underlying microscopic degrees of freedom lead to diffusive or relaxational spin dynamics at a given temperature range.

Recent progress in the strategic design of molecular-based single-chain magnets⁸⁻¹² (SCM's) and single-molecular magnets¹³ (SMM's) has opened a new window

on this problem. Among the SCM's are $[\text{Mn}(\text{saltmen})_2[\text{Ni}(\text{pao})_2(L)_2](A)_2$ (L , intrachain attaching ligand of Ni^{II} ion; A^{-1} , interchain counteranion),^{8,10,11} and $\text{Co}(\text{hfac})_2\text{NITPhOMe}$.⁹ In these materials, spin carriers exhibit a strong uniaxial (Ising) anisotropy to be able to block or freeze their magnetization in one direction. In the case of the SCM's, constituent spin chains are well isolated magnetically and finite-temperature phase transitions are not observed down to quite low temperatures. An essential difference between the SCM's and SMM's is characterized by the presence or absence of a correlation, respectively. The slow dynamics in SMM's is governed by the metastable intramolecular spin flipping, which leads to incoherent superparamagnetic slow relaxation. On the other hand, in the SCM's, elementary excitations and low-temperature dynamics are deeply influenced by many-body spin correlation. Actually, the SCM's exhibit a slow relaxation of zero-field ac magnetization with a single relaxation process.^{9-11,14} The importance of the ferromagnetic correlation was also made clear by ac-susceptibility measurements under pressure.¹⁴ In this material, at least 100 units of the Mn-Ni-Mn trimers form uniform chains¹¹ and no three-dimensional phase transition is observed down to quite low temperatures, at least $T > 40$ mK.¹⁰ Consistently, specific heat measurements show no signal of a phase transition.¹⁵ So this system serves as a nice example to investigate the slow dynamics in the paramagnetic phase and the situation is completely different from the slow dynamics originating from superparamagnetism or spin-glass phase transitions.

In this paper, to elucidate the low-energy excitations and the spin dynamics of the SCM, we report a NMR measurement of the spin dynamics of the heterometallic SCM $[\text{Mn}(\text{saltmen})_2[\text{Ni}(\text{pao})_2(\text{py})_2](\text{PF}_6)_2$. By combining the measurements of the dc susceptibility χ_0 , the ac susceptibility χ' , and the NMR relaxation rate T_1^{-1} , we obtain strong evidence that shows that correlated domains and DW motion govern the low-temperature spin dynamics of the SCM.

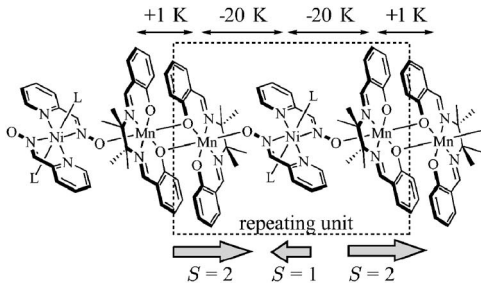


FIG. 1. The chain structure of the compound comprising the $[\text{Mn}^{\text{III}}\text{-Ni}^{\text{II}}\text{-Mn}^{\text{III}}]$ trimers.

II. EXPERIMENT

A. Crystal structure

We use polycrystalline samples of $[\text{Mn}(\text{saltmen})_2][\text{Ni}(\text{pao})_2(\text{py})_2](\text{PF}_6)_2$, prepared as described in Ref. 10. The total weight of the samples was 224 mg. This compound comprises of isolated heterometallic chains of Mn^{III} and Ni^{II} metal ions.¹⁰ As shown in Fig. 1, the chain consists of a repeated unit of the $[\text{Mn}^{\text{III}}\text{-Ni}^{\text{II}}\text{-Mn}^{\text{III}}]$ trimer, where the Mn^{III} and Ni^{II} carry spin $S=2$ and $S=1$, respectively. The counteranions PF_6^- are located between the chains. The intratrimer antiferromagnetic superexchange interaction between the Mn^{III} and Ni^{II} ions is estimated to be about $J_{\text{Mn-Ni}}/k_B \sim -21.5$ K, while the intertrimer ferromagnetic exchange interaction between the neighboring Mn^{III} ions is estimated to be about $J/k_B \sim 0.8$ K.¹⁰ At low temperatures $T \lesssim 2J_{\text{Mn-Ni}}$ (~ 40 K),¹⁶ the local intratrimer excitations are inactive and the system is regarded as an effective $S=3$ ferromagnetic chain with a strong Ising anisotropy.¹⁰ The elongation of O-Mn-O bonds along the chain causes Jahn-Teller distortion of Mn^{III} ,¹⁰ which gives rise to a large negative single-ion anisotropy $D \sim -2.5$ K parallel to the chain.¹¹ At low temperatures, this compound can be described as a chain of ferromagnetic coupled $S=3$ $[\text{Mn}^{\text{III}}\text{-Ni}^{\text{II}}\text{-Mn}^{\text{III}}]$ units.^{10,11}

B. dc and ac susceptibilities

The ac-susceptibility measurements with an ac-field amplitude of 3 Oe at frequency 100 Hz and the dc-susceptibility measurement were performed in the temperature region from 1.8 to 50 K and applied field $H=1.5, 2.0, 3.0, 4.0$ T, using a superconducting quantum interference device (SQUID) magnetometer (Quantum Design MPMS-5S) with an ac option. The results are presented together with the results of a theoretical analysis in Figs. 7(a) and 7(b), below.

C. NMR spectra and relaxation rate

The measurements of NMR were performed using the conventional phase-coherent pulsed-NMR spectrometer (PROT3001MR) produced by THAMWAY Inc. Field-swept spectra were obtained by recording the amplitude of the spin-echo signal. The spin-lattice relaxation rate T_1^{-1} was measured by the recovery of the magnetization with the integration intensity of the spin-echo signals.

First, we have measured ^{19}F -NMR spectra by observing a spin-echo signal as a function of an external field at a fre-

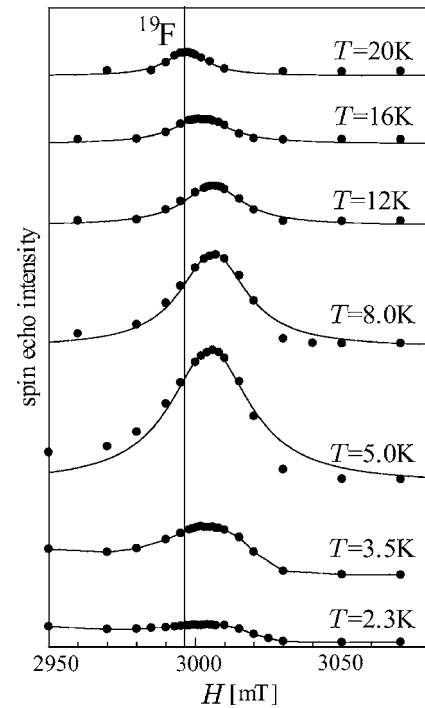


FIG. 2. Profile of field-swept ^{19}F NMR spectra for 120 MHz at different temperatures. The solid line indicates the free ^{19}F resonance field for 120 MHz.

quency of 63 MHz, 81 MHz, 120 MHz, and 157 MHz. Figure 2 shows field-swept spectra of ^{19}F -NMR at 120 MHz for selected temperatures. Similar behavior is also observed in the case at 63 MHz, 81 MHz, and 157 MHz. Above 20 K, only a sharp single line is observed around the free ^{19}F resonance field and the intensity increases with decreasing temperature. Below 20 K, the line becomes broad and the position of the peak shifts up to higher field around 8 K.

Second, we measured the spin-lattice relaxation rate T_1^{-1} at the field of the peak of the spectra. Figure 3 shows the recoveries of the intensity of a spin-echo signal of ^{19}F at $T=5.0$ K for 120 MHz. The recovery curve $M(t)$ is not single-exponential type but two-exponential-expression type with two spin-lattice relaxation rates $1/T_{1S}$ and $1/T_{1L}$ ($T_{1S} < T_{1L}$) as shown in Fig. 3. The solid line represents a two-exponential expression with $T_{1S}=0.88$ sec and $T_{1L}=1.8$ sec

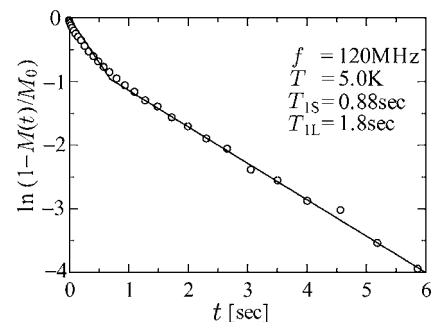


FIG. 3. A recovery of the intensity of a spin echo signal of ^{19}F for 120 MHz at $T=5.0$ K. The solid line shows a two-exponential expression with $T_{1S}=0.88$ sec and $T_{1L}=1.8$ sec.

as follows: $M(t) = M_S(1 - e^{-t/T_{1S}}) + M_L(1 - e^{-t/T_{1L}})$ where M_S and M_L are saturation recoveries with T_{1S} and T_{1L} , respectively. There are two F sites with different values spin-lattice relaxation times (T_{1S} and T_{1L}). However, the temperature and field dependence for T_{1L} is qualitatively the same as that for T_{1S} . The results are presented together with the results of theoretical analysis in Figs. 7 and 8, below.

III. THEORETICAL ANALYSIS

A. Low-lying excitation spectrum

Now, we attempt to theoretically analyze the low-energy dynamics response of the system. At present, however, it has not been definitely settled down whether the elementary excitations of the real $[\text{Mn}(\text{saltmen})_2][\text{Ni}(\text{pao})_2(\text{py})_2](\text{PF}_6)_2$ are truly dominated by Ising-like SCE or Heisenberg-like spin-wave excitations.^{17,18} To clarify this point, we first evaluate the low-lying excitation energies of a detailed quantum Hamiltonian,

$$\begin{aligned}
 H = & J_{\text{Mn-Ni}} \sum_{j=1}^L [\mathbf{S}_{3j-2} \cdot \mathbf{s}_{3j-1} + \mathbf{s}_{3j-1} \cdot \mathbf{S}_{3j}] \\
 & + J_{\text{Mn-Mn}} \sum_{j=1}^L [\mathbf{S}_{3j} \cdot \mathbf{S}_{3j+1}] + D_{\text{Mn}} \sum_{j=1}^L [(S_{3j-2}^z)^2 + (S_{3j}^z)^2] \\
 & + D_{\text{Ni}} \sum_{j=1}^L [(s_{3j-1}^z)^2], \quad (1)
 \end{aligned}$$

where \mathbf{S}_j (\mathbf{s}_j) is the spin-2 (spin-1) operator at the Mn (Ni) site. The ground state of this model has $S_{\text{tot}}^z = \pm 3L$. Since the system size dependence of the low-lying excitation energies is quite small, we can easily obtain the dispersion curves in the infinite-length limit, using numerical diagonalization of finite-size clusters up to $L=4$, with the periodic boundary condition. The lowest dispersion curves with $\delta S_{\text{tot}}^z = 1$ (one magnon), 2 (two magnons), 3 (three magnons), 4 (four magnons), and 6 (cluster excitation) calculated for the most suitable parameter sets [$J_F/J_{AF} = -0.07$, $D_{\text{Mn}}/J_{AF} = -0.27$, and $D_{\text{Ni}}/J_{AF} = 0$ (the effect of D_{Ni} is almost negligible)] are shown in Fig. 4. The cluster excitation corresponds to a flip of the $S=3$ object which consists of the Mn-Ni-Mn unit.

Figure 4 indicates that the excitations of more than two magnons has almost flat dispersions corresponding to the Ising-like SCE. We also show the S_{tot}^z dependence of the lowest excitation energy for $L=3$ and 4, as solid and dashed curves, respectively in Fig. 5. The right (left) edge corresponds to the ground state with $S_{\text{tot}}^z = \pm 3L$. Each step indicates the excitation energy for each value of S_{tot}^z , varying one by one along the curve. The cluster excitations correspond to $\delta S_{\text{tot}}^z = 6n$ ($n = \text{integer}$). Figure 5 indicates that a peak structure always appears between the two successive cluster excitations and the intermediate peak (except for a peak at the both edges) has completely the same form between $L=3$ and 4. It implies that this peak would be just repeated if the system size increases even up to much more. This repeated peak structure would correspond to the low-lying excitations of the $S=3$ Ising model with the effective anisotropies. Thus the

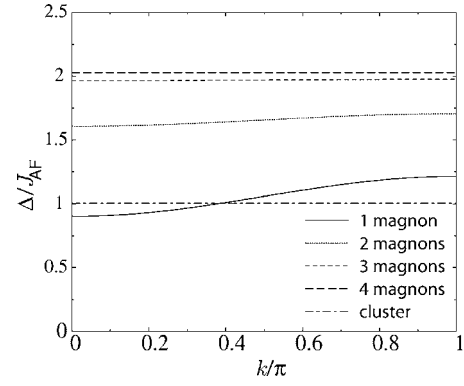


FIG. 4. Low-lying dispersion curves for one magnon, two magnons, three magnons, four magnons, and six magnons (cluster excitation), calculated by numerical exact diagonalization of finite-size clusters for the detailed Hamiltonian.

present system is expected to be effectively described by the $S=3$ Ising model at least at sufficiently low temperatures.

B. Analysis based on the one-dimensional Blume-Capel model

1. Transfer matrix analysis

Based on the above this observation, we are now ready to analyze the low-energy dynamic response of the infinite system.¹⁹ We use the one-dimensional $S=3$ Ising model as a “working assumption,” to simulate the low-energy dynamics of the single-chain magnet. In this sense, for temperatures above $2J_{\text{Mn-Ni}} \sim 40$ K, the intratrimer excitations are activated and the present assumption clearly breaks down. So we limit our treatment to the temperature window $T < 40$ K and how the low-temperature spin dynamics comes up to the physical quantities. By retaining the relevant terms indicated by the above-mentioned numerical analysis, we start with the one-dimensional $S=3$ Ising model with the single-ion anisotropy (Blume-Capel model):^{20,21}

$$\mathcal{H} = -2J \sum_{i=1}^L S_i^z S_{i+1}^z + D \sum_{i=1}^L (S_i^z)^2 - \tilde{H} \sum_{i=1}^L S_i^z, \quad (2)$$

where $S_i^z = 0, \pm 1, \pm 2, \pm 3$ represents the effective spin projection of the i th trimer, L denotes the number of the trimers,

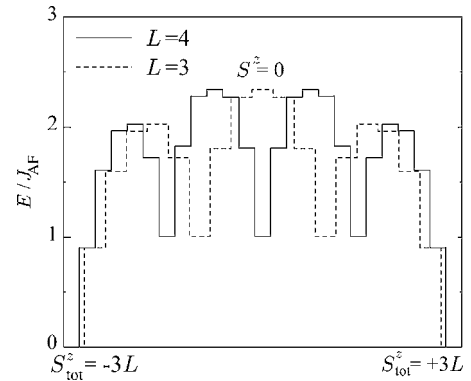


FIG. 5. Lowest excitation energies plotted versus S_{tot}^z for $L=3$ and 4, shown as dashed and solid curves, respectively.

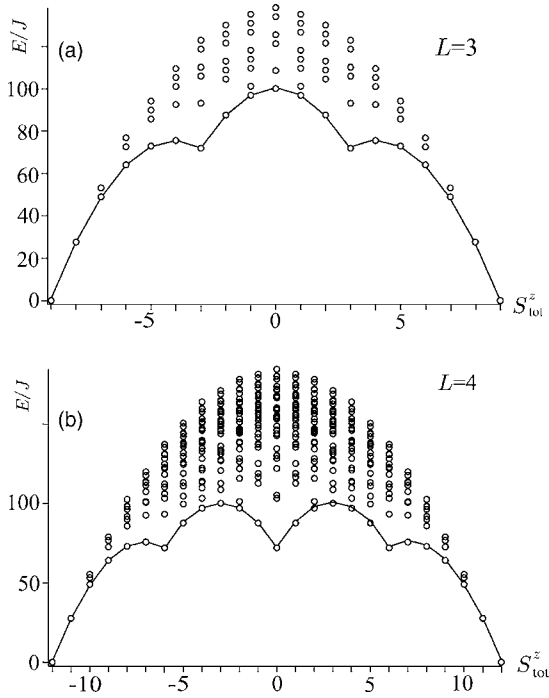


FIG. 6. Excitation spectrum of the effective model (2) as a function of the total spin $S_{\text{tot}}^z = \sum_{i=1}^L S_i^z$ for the cases of (a) $L=3$ and (b) $L=4$ with the periodic boundary condition. We set $D/J = -3.125$ (the same as those used to analyze the experimental data). The lower bounds of the spectrum are shown by the solid lines.

and $\tilde{H} = g\mu_B H$ represents an applied magnetic field.

In Fig. 6, we show the excitation spectrum of the effective model (2) as a function of total spin $S_{\text{tot}}^z = \sum_{i=1}^L S_i^z$ for the cases of $L=3$ and $L=4$ with the periodic boundary condition. We set $D/J = -3.125$, the same as those used to analyze the experimental data in the following section. The lower bounds of the spectrum are shown by the solid lines. It is clear that the spectra are qualitatively consistent with the result shown in Fig. 5 for the quantum Hamiltonian (1). This correspondence strongly supports that the present system is effectively described by the classical Hamiltonian (2).

The transfer matrix for the model (2) is given by $\mathbf{T}(S_i^z, S_{i+1}^z) = \exp[-\mathbf{H}(S_i^z, S_{i+1}^z)/k_B T]$, where

$$\mathbf{H}(S_i^z, S_{i+1}^z) = -2JS_i^z S_{i+1}^z + D(S_i^{z2} + S_{i+1}^{z2})/2 - \tilde{H}(S_i^z + S_{i+1}^z)/2.$$

Diagonalizing the 7×7 matrix \mathbf{T} leads to $\mathbf{T} = \sum_{\alpha=1}^7 |u_\alpha\rangle \lambda_\alpha \langle u_\alpha|$ with an eigenvector $|u_\alpha\rangle$ belonging to the eigenvalue λ_α . The exact partition function is given by $Z = \text{Tr}(\mathbf{T}^N) = \sum_{\alpha=1}^7 \lambda_\alpha^N$.

Next we consider the spin-spin correlation function $C_{ij} = \langle S_i^z S_j^z \rangle - \langle S_i^z \rangle \langle S_j^z \rangle$. Introducing the spin matrix $\mathbf{S} = \text{diag}(3, 2, 1, 0, -1, -2, -3) = \sum_{\alpha, \beta=1}^7 |u_\alpha\rangle \langle u_\alpha| \mathbf{S} |u_\beta\rangle \langle u_\beta|$, in the limit of $N \rightarrow \infty$ we obtain $\langle S_i^z S_j^z \rangle = \langle u_1 | \mathbf{S} | u_1 \rangle$ and

$$\langle S_i^z S_j^z \rangle = \langle u_1 | \mathbf{S} | u_1 \rangle^2 + \langle u_1 | \mathbf{S} | u_2 \rangle^2 (\lambda_2 / \lambda_1)^{j-i},$$

where λ_1 and λ_2 are the largest and second-largest eigenvalues of the transfer matrix, respectively, and $|u_1\rangle$ and $|u_2\rangle$ are

the eigenvectors belonging to λ_1 and λ_2 , respectively. We thus have the dc susceptibility

$$\chi_0 = \mu_B \langle u_1 | \mathbf{S} | u_1 \rangle / H, \quad (3)$$

with H being the applied magnetic field strength and the spin-spin correlation function $C_{ij} = B(T, H) (\lambda_2 / \lambda_1)^{j-i}$, where

$$B(T, H) = \langle u_1 | \mathbf{S} | u_2 \rangle^2. \quad (4)$$

We stress that the prefactor $B(T, H)$ has a strong T and H dependence. Since an explicit form of $B(T, H)$ as a function of T and H is not available here, we perform numerical evaluation after diagonalizing the transfer matrix. The correlation length is thus given by $\xi(T, H) = \{\log(\lambda_1 / \lambda_2)\}^{-1}$. The fluctuation-dissipation theorem gives the susceptibility

$$\chi' = C_0 / k_B T = B(T, H) \xi(T, H) / k_B T, \quad (5)$$

where C_0 represents the $q=0$ component of C_{ij} .

2. NMR ratio

The NMR relaxation rate is given by²²

$$T_1^{-1} = \frac{2\gamma_n^2}{(\gamma_e \hbar)^2} k_B T \lim_{\omega_N \rightarrow 0} \sum_q |A_q|^2 \frac{\text{Im} \chi_{zz}(q, \omega_N)}{\omega_N}, \quad (6)$$

where the dynamic susceptibility in the ω - q domain has the usual van Hove form $\chi_{zz}(q, \omega_N) = \chi_{zz}(q) / [i\omega_N \tau_q + 1]$.²³ Because of the Ising nature of the electron spins and the location of the ^{19}F nuclei, only the dipolar hyperfine coupling may become predominant. When we make an integration over q in Eq. (6), we retain only the uniform ($q=0$) component of τ_q . As for retaining only the $q=0$ component of the relaxation time, we are considering the relaxational dynamics and the relaxation ratio has always a constant term.¹ We note that in the case of the diffusive dynamics the q dependence is essential, but in the relaxational dynamics, a constant term plays a major role. We thus have $T_1^{-1} \sim T \chi' \tau(T, H) [\xi(T, H)]^{-d}$ with the spatial dimension $d=1$. The relaxational dynamics due to the random DW motion gives $\tau(T, H) \sim [\xi(T, H)]^z$, with $z=2$, and we have

$$T_1^{-1} \sim B(T, H) [\xi(T, H)]^{z-d+1}, \quad (7)$$

with $z=2$. Essentially the same expression has been obtained in the context of the spin fluctuations of highly correlated organic conductors.²⁴

IV. DISCUSSION

A. Dynamic response

Now, we discuss the experimental results based on the theoretical analysis presented in the preceding section. In Figs. 7(a), 7(b), and 7(c) we show the experimental data for the dc susceptibility χ_0 , ac susceptibility χ' , and the NMR relaxation rate T_1^{-1} , respectively, for the applied dc magnetic field strength $H=1.5, 2.0, 3.0, 4.0$ T. Theoretical fitting is done by using a single set of the dimensionless parameter $D/J = -3.125$ with $\tilde{H}/J = 1.875, 2.50, 3.75, 5.00$. Taking $J/k_B = 0.8$ K, this parameter choice is consistent with experi-

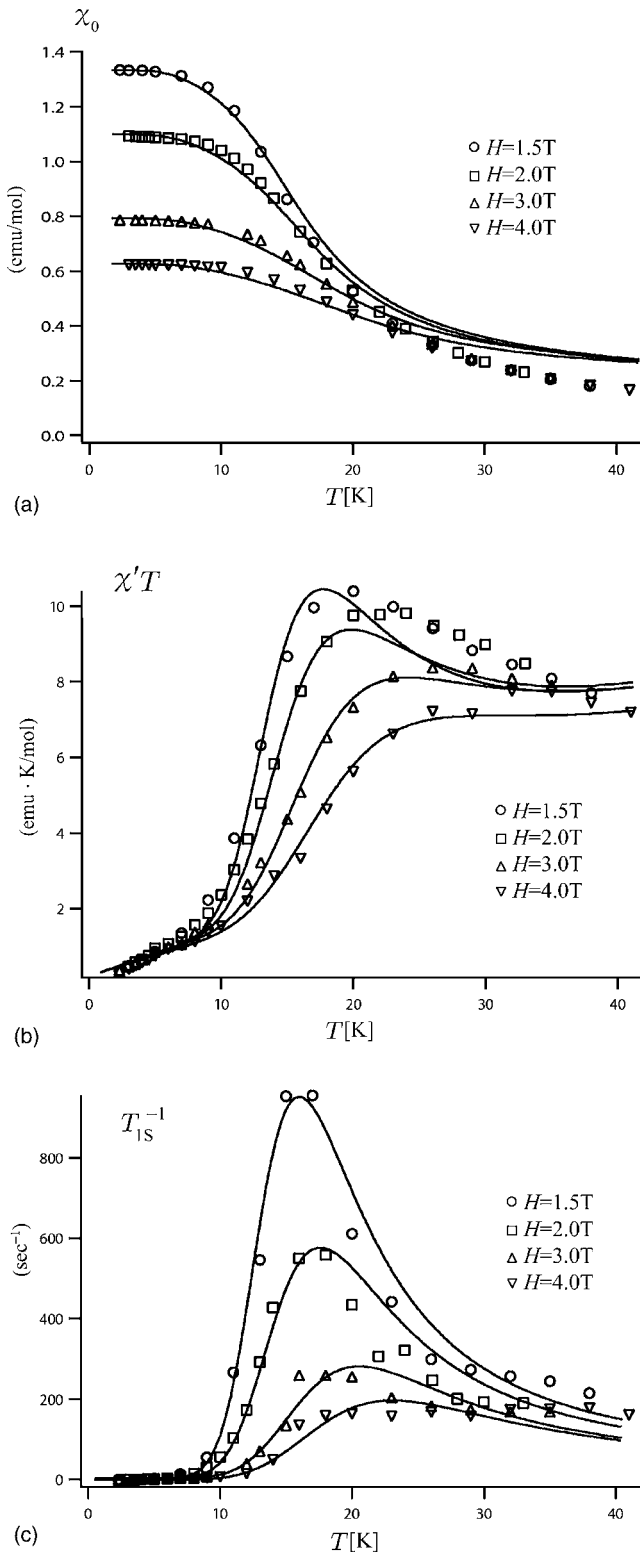


FIG. 7. The experimental data for the dc susceptibility χ_0 , ac susceptibility χ' , and the NMR relaxation rate T_{1S}^{-1} , respectively, for the applied dc magnetic field strength $H = 1.5, 2.0, 3.0, 4.0$ T. Fitting curves are given by Eqs. (3), (8), and (7), respectively.

mentally reported values ($J/k_B = 0.8$ K and $D/k_B = -2.5$ K).¹¹ We see that, at least for the low-temperature region, the theoretical curves are in good agreement with the experimental

ones. We here comment on the field strengths used in the experiments (for the polycrystalline samples) and theoretical analysis. In the experiments, these are the applied field strengths, whereas in Eq. (2) the longitudinal field (field in the anisotropy axis of the respective crystal) enters.

As we see in Fig. 7(a), the dc susceptibilities tend to saturate below $T \sim 10$ K. Since our samples are polycrystalline, the saturated magnetizations for different magnetic field strengths do not coincide with each other. Since there is no symptom of the phase transition over the temperature region observed here, this saturation indicates that the system approaches the zero-temperature criticality peculiar to the classical 1D system. We stress that if the intertrimer correlation does not exist, this type of saturation is never expected to occur.

In Fig. 7(b), we show the real part of the ac susceptibility χ' measured by the SQUID magnetometer. As the applied magnetic field strengths increase, the overall strengths of $\chi'T$ decrease and the peak temperature moves toward the higher-temperature sides. The theoretical fitting is done by the computed $\chi'T = B(T, H)\xi(T, H)$ with an additional constant term

$$\bar{\chi}' = a + B(T, H)\xi(T, H)/k_B T, \quad (8)$$

where a is independent of T and H . This constant shift is also observed in the zero-field ac measurement and at present its origin is not clear. The temperature and field dependence of $\bar{\chi}'$ comes mainly through the correlation length $\xi(T, H)$. It is to be noted that the prefactor B also has a strong T and H dependence. The broad maximum of $\chi'T$ mainly comes from the temperature dependence of the correlation length $\xi(T, H)$. The correlation length has a broad peak around the temperature, $T^* \sim \tilde{H}\xi(T, H)/k_B$. At temperatures lower than T^* , the correlated domains are easily polarized by the external magnetic field and then $\xi(T, H)$ plays a role as a “healing length.”

In Fig. 7(c), we show the spin-lattice relaxation rate $1/T_{1S}$ at the ^{19}F nuclei. Since the temperature and field dependences of the two relaxation times T_{1L} and T_{1S} are the same, we consider only the shorter one T_{1S} . Again, the theoretical fitting is done by the computed $T_{1S}^{-1} \sim B(T, H)[\xi(T, H)]^{z-d+1}$ with $z=2$ and $d=1$. We note that, as compared with $\chi'T$, the T_{1S}^{-1} acquires an additional contribution from the correlation length $\xi(T, H)$. Because of this, the peak temperatures of T_{1S}^{-1} shift toward the low-temperature sides as compared with those of $\chi'T$. Again we stress that this shift is never expected to occur if the intertrimer correlation does not exist, such as in the case of the SMM.²⁵ This result strongly supports the following evidence: (1) *the low-temperature magnetic responses are well understood by the temperature and field dependence of the correlation length ξ* , and (2) *the low-temperature dynamics is well described by the random motion of the DW's*. The second point is consistent with an idea that this system belongs to the Glauber-type (nonconserved relaxational) universality class.

Here we comment on reliability of treating polycrystalline sample by a simple Hamiltonian (2). In particular, a natural query arises about the transverse spin flipping processes. Regarding this point, in our experiment, the applied magnetic field is rather weak (up to 4 T). However, the single-ion

Ising-type anisotropy amounts to 30 K (this fact was confirmed by the ESR measurements).¹⁸ So the magnetic field strengths are not sufficient to cause transverse spin fluctuations. As long as the transverse spin flipping processes are inactive, only the longitudinal degrees of freedom are active and the resulting Hamiltonian contains only the longitudinal (S^z) components and temperature dependence of the response functions are insensitive to the relative direction of the sample with respect to the external field. This situation justifies using a simple Hamiltonian (2).

B. Diffusive dynamics and relaxational dynamics

Finally, we pay attention to the field dependence of T_1^{-1} . When the spin-wave-driven diffusive dynamics dominates the DW-driven relaxational dynamics, the correlated precession of the spins around the applied magnetic field give rise to the transverse spin-spin correlation function

$$C_{xx}(q,t) \propto \exp(-\Gamma_q t) \exp(-i\omega_e t), \quad (9)$$

with $\Gamma_q = \Gamma q^2$ for small q , where Γ denotes the spin diffusion constant and $\omega_e = g\mu_B H/\hbar$ denotes the electron Larmor frequency. In 1D, this leads to the characteristic field dependence of T_1 as²⁶

$$T_1^{-1} \propto 1/\sqrt{H}. \quad (10)$$

On the other hand, in the case of the relaxational dynamics without precession, $\Gamma_q = \text{const}$ and ω_e does not enter the spin-spin correlation function, and consequently T_1^{-1} is almost independent of H . As we seen in Fig. 8, we clearly see that in the higher-temperature regime, a linear $1/\sqrt{H}$ dependence of T_{1S}^{-1} is observed, indicating a crossover behavior from the relaxational to diffusive dynamics. As the temperature increases, the thermal fluctuations dominate the single-ion anisotropy energy and the system tends to be described by the anisotropic Heisenberg magnet,¹⁷ where the spin-wave excitations become predominant.

V. CONCLUDING REMARKS

In conclusion, we made the report of the combined measurements of the dc susceptibility χ_0 , the ac susceptibility χ' ,

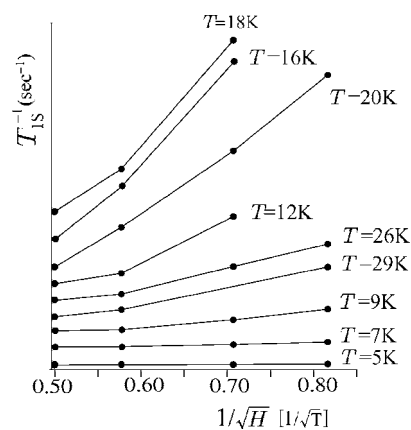


FIG. 8. The same data of T_{1S}^{-1} as Fig. 4 are plotted against $1/\sqrt{H}$. The curves are shifted parallel to the vertical axis to make the $1/\sqrt{H}$ dependence easy to see.

and the NMR relaxation rate T_1 for the single-chain magnet. By evaluating the low-lying excitation energies of a detailed finite-size Hamiltonian, we found that the present system is effectively described by the $S=3$ Ising model at least at sufficiently low temperatures. Based on this observation, we used the infinite-size one-dimensional $S=3$ Ising model as a “working assumption” to simulate the low-energy dynamics of the single-chain magnet. The corresponding 1D $S=3$ Ising model with the single-ion term (Blume-Capel model) was exactly solved by the transfer-matrix method. Assuming that the low-temperature dynamics is governed by the random motion of the local domain walls, we qualitatively reproduced the experimental results by using a single parameter set. We may, therefore, reasonably conclude that this system is, at least qualitatively, a good laboratory realization of the correlated one-dimensional classical spin systems.

ACKNOWLEDGMENTS

We acknowledge fruitful communications with H. Nojiri and Y. Nakazawa. J.K. acknowledges helpful discussions with Y. Itoh, K. Minami, and H. Fukuyama.

¹P. C. Hohenberg and B. I. Halperin, Rev. Mod. Phys. **49**, 435 (1977).

²R. J. Glauber, J. Math. Phys. **4**, 191 (1963).

³M. Date and M. Motokawa, Phys. Rev. Lett. **16**, 1111 (1966).

⁴M. Steiner, J. Villain, and C. G. Windsor, Adv. Phys. **25**, 87 (1976).

⁵F. Borsa and A. Rigamonti, in *Magnetic Resonance of Phase Transitions*, edited by F. J. Owens, C. P. Poole, and H. A. Farach (Academic Press, New York 1979), p. 79.

⁶E.g., J. P. Boucher, H. Benner, F. Devreux, L. P. Regnault, J. Rossat-Mignod, C. Dupas, J. P. Renard, J. Bouillot, and W. G. Stirling, Phys. Rev. Lett. **48**, 431 (1982).

⁷H. Seitz and H. Benner, Z. Phys. B: Condens. Matter **66**, 485 (1987).

⁸R. Clérac, H. Miyasaka, M. Yamashita, and C. Coulon, J. Am. Chem. Soc. **124**, 12837 (2002).

⁹A. Caneschi, D. Gatteschi, N. Lalioti, C. Sangregorio, R. Sessoli, G. Venturi, A. Vindigni, A. Rettori, M. G. Pini, and M. A. Novak, Europhys. Lett. **58**, 771 (2002).

¹⁰H. Miyasaka, R. Clérac, K. Mizushima, K. Sugiura, M. Yamashita, W. Wernsdorfer, and C. Coulon, Inorg. Chem. **42**, 8203 (2003).

¹¹C. Coulon, R. Clérac, L. Lecren, W. Wernsdorfer, and H. Miyasaka, Phys. Rev. B **69**, 132408 (2004).

¹²T. Kajiwara, M. Nakano, Y. Kaneko, S. Takaishi, T. Ito, M. Yamashita, A. I. Kamiyama, H. Nojiri, Y. Ono, and N. Kojima, J. Am. Chem. Soc. **127**, 10150 (2005).

- ¹³D. Gatteschi and R. Sessoli, *Angew. Chem., Int. Ed.* **42**, 268 (2003).
- ¹⁴M. Mito, H. Deguchi, T. Tajiri, S. Takagi, M. Yamashita, and H. Miyasaka, *Phys. Rev. B* **72**, 144421 (2005).
- ¹⁵Y. Nakazawa (private communication).
- ¹⁶The lowest excitation energy of an isolated $[\text{Mn}^{\text{III}}\text{-Ni}^{\text{II}}\text{-Mn}^{\text{III}}]$ trimer amounts to $2J_{\text{Mn-Ni}} \sim 40$ K (Ref. 10).
- ¹⁷T. Sakai, M. Matsumoto, K. Asakura, and M. Sato, *Prog. Theor. Phys. Suppl.* **159**, 308 (2005).
- ¹⁸Y. Oshima, H. Nojiri, K. Asakura, T. Sakai, H. Miyasaka, and M. Yamashita, *Phys. Rev. B* **73**, 214435 (2006).
- ¹⁹In the real $\text{Mn}^{\text{III}}\text{-Ni}^{\text{II}}\text{-Mn}^{\text{III}}$, it is reported that at least 100 units of the Mn-Ni-Mn trimers form uniform chains (Ref. 11). This situation is qualitatively well described by the Hamiltonian for the system of infinite size.
- ²⁰M. Blume, *Phys. Rev.* **141**, 517 (1966).
- ²¹H. W. Capel, *Physica (Utrecht)* **32**, 966 (1966); **33**, 295 (1967).
- ²²T. Moriya, *J. Phys. Soc. Jpn.* **18**, 516 (1963).
- ²³This form directly gives the spin-spin correlation function in the t - q domain that decays in a form $\chi_{zz}(q)e^{-|q|\tau_q}$.
- ²⁴C. Bourbonnais, P. Wzietek, F. Creuzet, D. Jerome, P. Batail, and K. Bechgaard, *Phys. Rev. Lett.* **62**, 1532 (1989).
- ²⁵P. Santini, S. Carretta, E. Livioti, G. Amoretti, P. Carretta, M. Filibian, A. Lascialfari, and E. Micotti, *Phys. Rev. Lett.* **94**, 077203 (2005).
- ²⁶D. Hone, C. Scherer, and F. Borsa, *Phys. Rev. B* **9**, 965 (1974).